ACS Sustainable Chemistry & Engineering

Research Article

pubs.acs.org/journal/ascecg

# Carbon Dioxide Capturing by Nitrogen-Doping Microporous Carbon

Pei Li,[†,‡] Chuang Xing,[§] Shijie Qu,[†] Bin Li,[∥] and Wenzhong Shen*[,†]

[†]Institute of Coal Chemistry, Chinese Academy of Sciences, Taiyuan, Shanxi 030001, People's Republic of China

[‡]University of Chinese Academy of Sciences, Beijing 100049, People's Republic of China

[§]Zhejiang Provincial Key Lab for Chem. & Bio. Processing Technology of Farm Product, School of Biological and Chemical Engineering, Zhejiang University of Science and Technology, Hangzhou 310023, People's Republic of China

[∥]Zhengzhou Tobacco Research Institute of China National Tobacco Corporation, Zhengzhou 450001, People's Republic of China

Supporting Information

**ABSTRACT:** Nitrogen-containing microprous carbon was successfully synthesized by using phloroglucinol and glutaraldehyde as the carbon source and hydrolyzed silk as the nitrogen source. The porous structures and surface chemical compositions of microporous carbon were analyzed and characterized by nitrogen adsorption isotherms, thermogravimetric analysis, Fourier transform infrared spectrum and scanning electron microscope images. The resultant porous carbons had a microporous structure, and the pore size distribution was 0.7−2.0 nm. Phenolic formaldehyde with silk was pyrolyzed and decomposed to condense a cross-linking structure between 230 and 650 °C. The nitrogen-containing groups from silk decomposition were incorporated into a carbon matrix during the carbonization process. The microporous carbon showed good regeneration performance and high adsorption capacities of $CO_2$ due to its nitrogen-containing groups and developed a micropore structure. Under dynamic conditions, $CO_2$ could be finely separated from a mixture of $CO_2$, $N_2$ and $CH_4$ with microporous carbon, which displayed potential application for $CO_2$ capture.

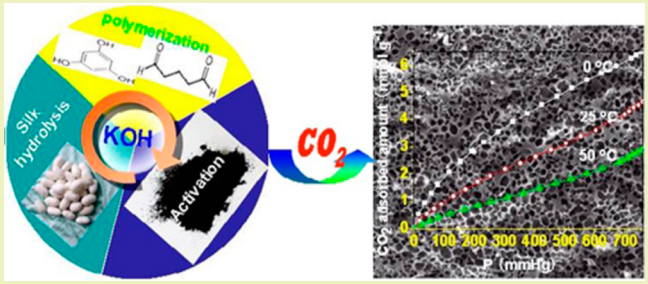


**KEYWORDS:** *Phloroglucinol, Glutaraldehyde, Silk, KOH activation, $CO_2$ adsorption, Separation*

## INTRODUCTION

Porous carbons are generally utilized as adsorbents,[1−3] catalyst supports[4] and energy storage materials,[5] due to its well-developed pore structure (high specific surface areas, large pore volumes). They are usually derived from carbon precursors by carbonization and/or associating with activation or templating technology.[6] The chemical activation could effectively promote pore formation and development; KOH, NaOH, $H_3PO_4$ and $ZnCl_2$[7,8] are usually selected as activation agents. Porous carbon with a developed pore structure could be obtained by chemical activation at lower temperatures and shorter activation times. A narrower micropore distribution of porous carbon can be prepared using KOH activation.[9] The surface areas of graphene,[10] carbon nanotubes,[11] carbide-derived carbon and mesoporous carbon[12] could be increased by KOH activation, and their electrochemical performances were improved.

In general, the application property of porous carbon was determined by its pore structure and surface chemical groups. However, the surfaces of porous carbons are hydrophobic and contain few functional groups because of carbonization or activation at high temperatures. The surface hydrophilicity of porous carbon could be enhanced when heteroatoms (oxygen, nitrogen, sulfur, etc.) were incorporated into a carbon matrix.[13−15] Thus, its adsorption properties for polar molecules could be improved.[16] Nitrogen-rich precursors, such as acrylonitrile,[17] melamine,[18] cyanamide,[19] ethidene diamine[20] and amide-containing molecular cages,[21] are always selected to fabricate nitrogen-containing porous carbon. Generally, bulk carbon materials with desirable porosity could be prepared by directly carbonizing these precursors.[22] However, these carbon precursors are expensive and the exhausts are hazardous to the environment.

Nitrogen-doping is an effective method to obtain nitrogen-containing porous carbon. Various nitrogen-doping porous carbons have been reported, such as porous carbon monoliths,[23] carbon nitride spheres,[15] organic molecular materials,[24] imidazolate frameworks,[25] amine-modified silica,[26] amine-modified MFI membranes,[27] fibers[28] and carbon nanosheets.[29] Nitrogen-doping needs expensive nitrogen-rich precursors or doping at high temperatures; moreover, the doped nitrogen content is much lower. So, it is necessary to develop a novel and facile method to introduce nitrogen-containing groups into a carbon matrix.

The concentration of carbon dioxide has increased in the atmosphere and it has been postulated as an important factor of global climate change. Solution absorption, adsorption by

Received: March 3, 2015
Revised: May 31, 2015
Published: June 10, 2015





DOI: 10.1021/acssuschemeng.5b00291
ACS Sustainable Chem. Eng. 2015, 3, 1434−1442

porous materials, membrane separation and cryogenics are being developed for $CO_2$ separation and capture. Among them, adsorption is a potential technology on a large scale due to its low energy consumption and operation cost. The adsorption amount and selectively of $CO_2$ are the most important criteria for evaluation of an adsorbent.

Herein, we synthesized a nitrogen-containing microporous carbon with developed pore structure using phloroglucinol and glutaraldehyde as carbon sources and silk as a nitrogen source. KOH was adopted as a catalyst for polymerization of phloroglucinol with glutaraldehyde and activation agent to promote micropore forming during activation. The synthetically nitrogen-doped porous carbon exhibits a high amount of $CO_2$ adsorption and good separation from $N_2$−$CO_2$, $CH_4$−$CO_2$ due to its well-developed pore structure and richness of nitrogen-containing groups.

## EXPERIMENTAL SECTION

**Synthesis of Porous Carbon.** Cocoons of *Bombyx mori* silkworm silk were boiled in 5 wt % $Na_2CO_3$ solution for 1 h and then washed by distilled water to remove sericin proteins. The treated silk was impregnated into a KOH solution (mass ratio of silk to KOH was 1:1) for 0.5 h, and the mixture of silk and KOH solution was added into a 100 mL Teflon-lined autoclave and heated at 180 °C for 12 h. Then the autoclave naturally cooled back to ambient temperature, and a brown red silk hydrolysis solution was obtained.

Nanoporous carbon was fabricated by phloroglucinol and glutaraldehyde copolymerizing; hydrolyzed silk and KOH were selected as the nitrogen source and activation agent. The mass composition of the mixture was phloroglucinol/glutaraldehyde/KOH/silk = 9:10.7:1:7. In a typical procedure, 4 mmol phloroglucinol was dissolved in 5 mL of deionized water, 6 mmol glutaraldehyde (50 wt %) was added and the mixture was stirred for 5 min. Then 4 mL of a silk hydrolysis solution (containing 5 mmol KOH) was added, and the mixture was stirred at 80 °C in a water bath. A cross-linking phenol formaldehyde resin framework with silk and KOH was obtained within 10 min and dried at 110 °C for 6 h. The dried sample (noted as PFS) was carbonized at 600 or 800 °C for 1 h with a 5 °C/min heating rate in a $N_2$ flow of 50 mL/min. The obtained samples were rinsed with excessive amounts of 2 M HCl aqueous solution, followed by hot distilled water to remove chloride ions. Finally, these materials were dried at 120 °C. The resultant samples were designated as PFS-600 and PFS-800 (600 and 800 represent the carbonization temperature). For comparison, silk with KOH (the mass ratio of 1:1, named as S-KOH), resultant phenol formaldehyde resin from phloroglucinol and glutaraldehyde with KOH (the mass ratio of 1:1, named as PF-KOH) were treated at 800 °C by the same process, and the resultant samples were denoted as S-800 and PF-K-800. To illustrate the role of nitrogen-containing groups on $CO_2$ adsorption, PFS-600-HCl and PFS-800-HCl were treated with 37 wt % HCl and stirred for 24 h to neutralize totally the basic sites. Then the treated samples were rinsed with abundant water after the filtrate was neutral; the samples were dried at 110 °C for 12 h and named as PFS-600-HCl and PFS-800-HCl.

**Characterization.** Nitrogen adsorption−desorption isotherms of as-prepared samples were measured at −196 °C by a Micromeritics ASAP 2020 adsorption apparatus. The adsorption branch isotherms were adopted to calculate the surface areas and pore size distributions of samples using the Brunauer−Emmett−Teller (BET) method ($P/P_0$ of 0.01 to 0.2) and the nonlocal density functional theory (NLDFT) method (slit pore model). The total pore volumes ($V_{total}$) were counted based on the adsorption amount at $P/P_0$ of 0.99. The SEM images were observed using an S-4800 field emission-scanning electron microscope (Hitachi, Japan) manipulated at 1 kV. Fourier transform infrared (FT-IR) spectra of samples were obtained by a Nicolet FT-IR 380 spectrometer using the KBr pellet technique. Thermogravimetric analysis was carried out under Ar flow from 30 to 800 °C with a 10 °C/min heating rate by a thermogravimetric analyzer (Rigaku, TG-DTA 8120, Japan), and the exhausted gases were detected by consequent mass spectroscopy (Omni Star). The X-ray photoelectron spectra (XPS) were recorded with an ESCALAB 250 (Thermo Electron); the X-ray excitation was provided by a monochromatic Al K$\alpha$ (1486.6 eV) source. Survey scans were received using a 100 eV pass energy, whereas high-resolution scans of specific elements were obtained using a 20 eV pass energy. The emitted photoelectrons were detected by performing perpendicular to the surface sample. Data quantification was achieved by the advantage program.

**$CO_2$ Capture and Separation.** The $CO_2$ adsorption isotherms of porous carbons at different temperatures were examined by a Micromeritics ASAP 2020 static volumetric analyzer. Prior to each adsorption, the sample was degassed at 150 °C for 2 h to ensure the residual pressure less than $5 \times 10^{-3}$ mbar and then cooled to 25 °C, and $CO_2$ was provided into the system. The $CO_2$-adsorption capacity was calculated on the basis of adsorbed volume under standard temperature and pressure.

$CO_2$ temperature-programmed desorption profiles ($CO_2$-TPD) were investigated on a Bel Japan TPD-1-AT apparatus with a quadrupole mass detector. Prior to $CO_2$-TPD experiment, the samples (50 mg) were heated in situ at 300 °C for 1 h and cooled to 25 °C under He flow of 50 mL/min and then kept under He flow for 30 min. $CO_2$ (20 mL/min) was imported at 25 °C for 60 min, and the samples were kept again under He flow of 50 mL/min for 30 min to remove the free $CO_2$. Then the samples were heated to 300 °C at a rate of 10 °C/min under He gas flow, and the desorption of $CO_2$ was monitored.

The separation properties of $CO_2$ from $CO_2$−$N_2$ and $CO_2$−$CH_4$ mixtures were examined in a fixed-bed flow sorber (stainless steel tube, 9 mm in inner diameter and 100 mm in length, 330 mg sample) performed at ca. 1 atm and 25 °C. The sorbent bed was heated to 200 °C in Ar at a flow rate of 100 mL/min and kept for 30 min. Breakthrough experiment was operated by switching abruptly from Ar to a gas mixture of $CO_2$−$N_2$ or $CO_2$−$CH_4$ with the $CO_2$ concentration of 10−16 vol % at a flow rate of 12 mL/min. The treated gas from the sorber was monitored online by an Agilent 7890A gas chromatograph with a TCD detector.

## RESULTS AND DISCUSSION

The thermal gravimetric curves and exhausted gases of silk with KOH (S-KOH), PF with KOH (PF-KOH) and PFS were investigated to understand its thermal behaviors. Figure 1 displays their weight loss with temperature. For PF-KOH, the initial stage of weight loss (10 wt %) occurred from 50 to 200 °C, which could be ascribed to the adsorbed and bound water vanishing. The second weight loss stage, which was also the highest one (ca. 50 wt %), appeared between 200 and 350 °C with the fastest weight loss rate due to degradation of PF-KOH.

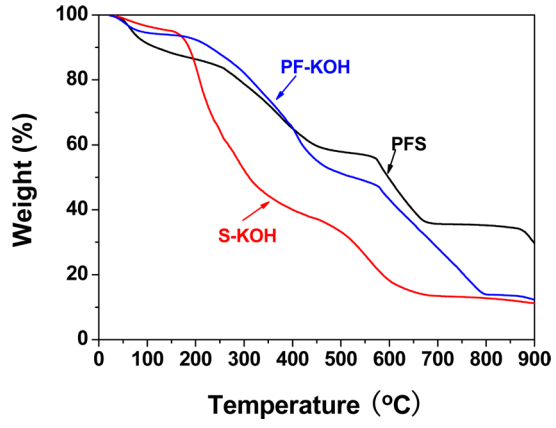


**Figure 1.** Thermogravimetric curves plots of S-KOH, PF-KOH and PFS.



DOI: 10.1021/acssuschemeng.5b00291
*ACS Sustainable Chem. Eng.* 2015, 3, 1434−1442

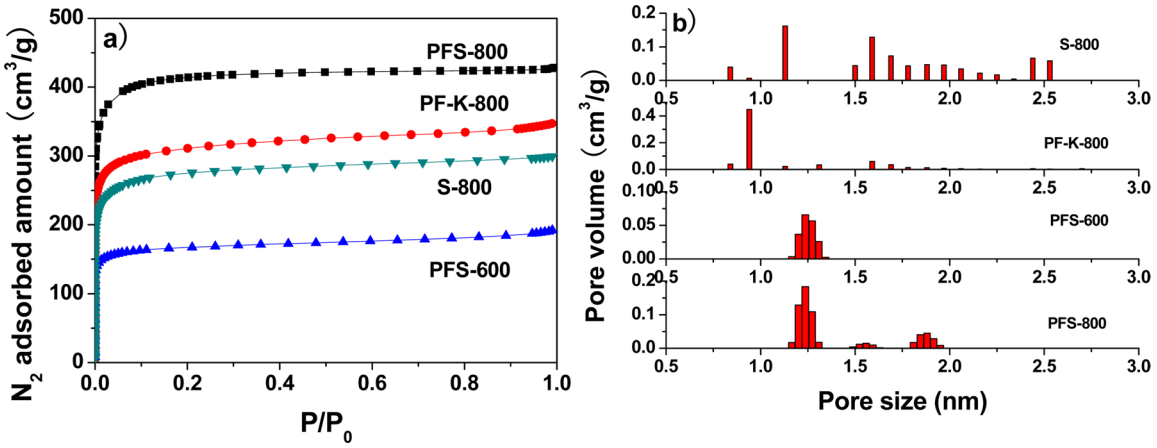


**Figure 2.** (a) $N_2$ adsorption isotherms; (b) NDFT pore size distributions of PFS-800, PFS-600, PF-K-800 and S-800.

**Table 1. Structure Parameters and Chemical Composition of Samples**

| | structure parameters | | | | elemental composition (wt %)[d] | | |
|---|---|---|---|---|---|---|---|
| samples | $S_{BET}$ ($m^2/g$)[a] | $S_{Micro}$ ($m^2/g$)[b] | $V_{Total}$ ($cm^3/g$)[c] | $V_{Micro}$ ($cm^3/g$) | N | H | C |
| PFS-800 | 1272 | 749 | 0.648 | 0.377 | 1.75 | 0.72 | 87.88 |
| PFS-600 | 576 | 560 | 0.297 | 0.236 | 4.07 | 2.62 | 80.13 |
| S-800 | 928 | 895 | 0.473 | 0.376 | 3.20 | 1.19 | 86.92 |
| PF-K-800 | 1083 | 1042 | 0.537 | 0.435 | | 1.55 | 92.73 |

[a]Specific surface area was calculated by the BET method. [b]Micropore surface area was derived from the *t*-plot method. [c]Total pore volume was obtained at $P/P_0$ = 0.99. [d]Data were from elemental analysis.

The weight loss rate slowed down when the temperature reached higher than 350 °C. In this stage, PF-KOH continued to decompose and form a condensed cross-linking structure. The degradation behavior of PFS-KOH was different from that of PF-KOH. The weight loss at temperatures lower than 150 °C was the removal of adsorbed water. The beginning degradation temperature appeared at ca. 250 °C because of silk decomposing and phenolic resin pyrolysis; the drastic weight loss occurred between 570 and 770 °C due to further release of gaseous products. The weight loss of S-KOH at 400 and 600 °C exceeded 60 and 90 wt %, respectively. As a natural protein, silk could be pyrolyzed and easily reacts with KOH at high temperatures. The yields based on carbon precursors of PF-KOH, S-KOH and PFS were 14.2 wt %, 12.7 and 35.2 wt % at 800 °C, respectively. The exhausted gases of PF-KOH, PFS and S-KOH during pyrolysis were mainly $H_2O$, CO and $CO_2$, and detailed information is shown in Figure S1 of the Supporting Information. The intensity of $H_2O$ that came from desorption of water at low temperature and decomposition and pyrolysis of silk, phenolic resin at high temperature was much higher than that of other gases for all the samples. $CO_2$ was formed between 280 and 500 °C, and CO appeared at temperatures higher than 430 °C. The nitrogen content was 17 wt % in silk; hydrocyanic acid (HCN) was formed by the pyrolysis and decomposition of silk and appeared from 440 to 520 °C.

The $N_2$ adsorption−desorption isotherms of PFS-600, PFS-800, PF-K-800 and S-800 are shown in Figure 2a; they exhibited type I adsorption isotherms, which is typically observed on microporous solids. The pore size distributions derived from the adsorption branch of nitrogen adsorption isotherms using the NLDFT method are illustrated in Figure 2b. It demonstrated the presence of micropores in the range of 1−2 nm. The primary pore structure parameters of samples are listed in Table 1. The specific surface area and pore volume of PFS-600 were 576 $m^2/g$ and 0.297 $cm^3/g$, and its micropore was concentrated at ca. 1.1 nm. Compared with PFS-600, PFS-800 had a higher specific surface area of 1272 $m^2/g$ and larger pore volume of 0.648 $cm^3/g$, and possessed micropores of 1.10−1.74 nm, which showed the effectiveness of KOH in generation of micropores in a carbon matrix at high temperatures, the reaction activity and rate between carbon and KOH rapidly increased with temperature. However, nitrogen content in resultant porous carbon decreased with temperature, the nitrogen content of PFS-600 was 4.75 wt % and that of PFS-800 was 1.75 wt % (Table 1), indicating that above 600 °C, the activation process was enhanced and nitrogen was eliminated by transforming into nitric oxide or other gases.[30] Meanwhile, PF-K-800 also displayed high surface area of 1083 $m^2/g$ and pore volume of 0.53 $cm^3/g$ and micropore mainly distributed 1.3−2.0 nm. The pore size distribution of S-800 is more scattered than that of others, and it appeared at 2.6 nm. In this work, KOH took three roles: catalytic hydrolysis of silk, catalytic polymerization of phloroglucinol and glutaraldehyde, as an activation agent for micropore formation during carbonization processing.

The morphologies of PFS, PFS-600 and PFS-800 are shown in Figure 3. The surface of PFS was dense and coarse, and a significant amount of pores could be observed on the surfaces of PFS-600 and PFS-800. Moreover, the porous structure of PFS-800 suggested that KOH could promote pore forming and more carbon was burnt off at high temperatures. The morphologies of S-800 and PF-K-800 are also shown in Figure S2 of the Supporting Information; S-800 consisted of little particles due to the poor thermal stability of silk and burnt off by KOH, whereas PF-800 had holes with diameters of micrometer scale size.


DOI: 10.1021/acssuschemeng.5b00291
ACS Sustainable Chem. Eng. 2015, 3, 1434−1442

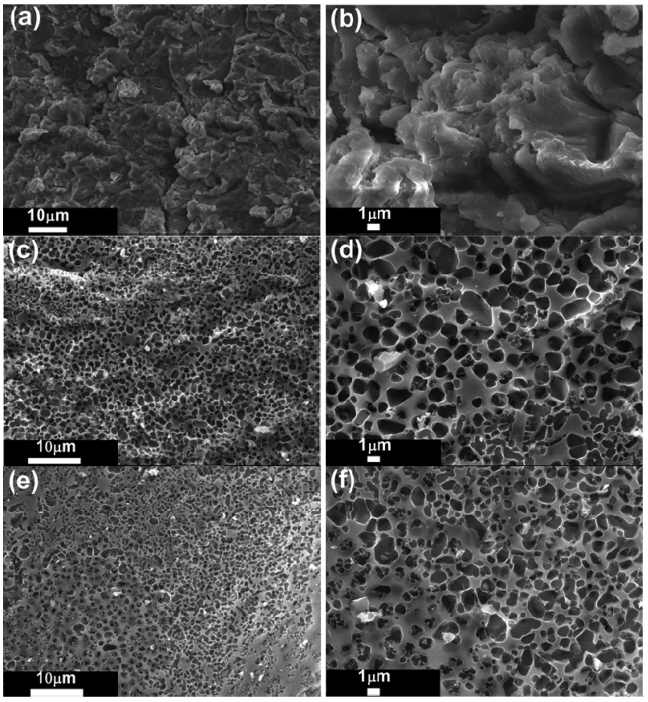


**Figure 3.** SEM images of PFS (a, b), PFS-600 (c, d) and PFS-800 (e, f).

Fourier transform infrared (FT-IR) spectra of PF, PFS, PF-K-800, PFS-600, PFS-800 and S-800 are shown in Figure 4.

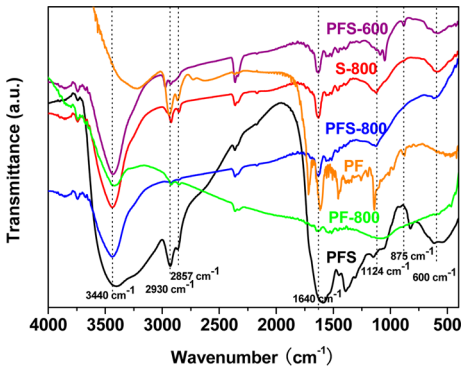


**Figure 4.** FT-IR spectra of PFS-800, PFS-600, PFS, S-800, PF and PF-K-800.

Compared with PFS, the intensities of absorption bands of PFS-600 and PFS-800 were decreased with carbonization temperature. A strong and broad band appeared around 3440 $cm^{-1}$ was ascribed to −OH symmetric stretching, indicating phenolic −OH or N—H symmetric stretching existing in PFS-600 and PFS-800.[31] The two bands appearing from 2800 to 3000 $cm^{-1}$ were the saturated bonds C—H stretching.[23] The band around 1640 $cm^{-1}$ was attributed to C═C stretching in PFS-600 and PFS-800, and the band around 1400 $cm^{-1}$ belonged to the C—H group stretching vibration of $-CH_2OH$.[32] Furthermore, the weak bands at 1124 and 875 $cm^{-1}$ suggested the presence of the C—N species and s-triazine ring in the carbon matrix, respectively.[33] The deformation vibration of $-NH_2$ could be identified by the abroad band at 600 $cm^{-1}$.[23] The FT-IR analysis confirmed that C—N and N—H species existed in PFS-600 and PFS-800. These absorption bands at 3440, 2930, 2867, 1640 and 1124 $cm^{-1}$ were ascribed to N—H, C—H, C═C and C—N groups in S-800. Although the intensities of absorb bands of PF-K-800 were much weaker than those of others, it illustrated that there were fewer chemical groups on its surface.

X-ray photoelectron spectroscopy (XPS) was conducted to confirm chemical compositions on PFS-600 and PFS-800 surfaces. As shown in Figure 5, the typical binding energies patterns of N 1s and O 1s appeared in the XPS spectra for PFS-600 and PFS-800. Four types of nitrogen configurations as pyridine-like nitrogen (N-6, 398.4 ± 0.1 eV), pyrrole-like nitrogen (N-5, 400 ± 0.1 eV), graphite-like nitrogen (N-Q, 401.3 ± 0.2 eV) and pyridine-*N*-oxide (N-X, 403.1 ± 0.2) are illustrated in Figure 5a,b. The nitrogen contents of four peaks from deconvolution of the N 1s spectra are listed in Table 2. The relative peak areas of N-6, N-5, N-Q and N-X for PFS-600 and PFS-800 were 1.00:1.98:0.88:0.26 and 1.00:1.02:0.80:0.23, respectively. There was a slight decrease in the N-5 peaks (from 50.6% of PFS-600 to 48% of PFS-800), whereas there were modest increases in the N-Q and N-X species. In addition, N-6 and N-5 species were principal, 75.3% and 72.2% fraction of PFS-600 and PFS-800, respectively. This discrepancy was in agreement reports that the nitrogen chemical groups were reduced at high activation temperatures.[34] XPS analysis also indicated that partial oxygen atoms were adhered to carbon surface, they mainly came from the introduced oxygen during activation by KOH, and the absorbed oxygen and/or water in air as well. O 1s peaks of PFS-600 and PFS-800 are shown in Figure 5c,d. The binding energies around 530.9, 531.9 and 533.3 eV demonstrated C═O, C—OH and/or C—O—C ether groups, chemisorbed oxygen and/or water, respectively.[35] The relative contents of different oxygen-containing groups are listed in Table S1 of the Supporting Information. The C 1s XPS spectra of PFS-600 and PFS-800, displayed rather complex deconvolution patterns (Figure S3 of the Supporting Information). The primary peak at 284.6 eV corresponded to the graphitic carbon, suggesting that most of the C atoms were arrayed in conjugated hexagon lattices.

The above characterizations confirmed oxygen and nitrogen-containing groups existing in PFS-600 and PFS-800, and there was no nitrogen-containing groups in PF-K-800. The adsorption isotherms of $CO_2$ for PFS-600, PFS-800, PF-K-800 and S-800 are drawn in Figure 6; the $CO_2$ uptakes were 4.62, 3.65, 3.78 and 3.27 mmol/g for PFS-800, PFS-600, PF-K-800 and S-800 at 25 °C and 1 atm, respectively. S-800 had a higher surface area and larger pore volume than that of PFS-600, but its $CO_2$ adsorption capacity was less than that of PFS-600 because of its more scattered pore size distribution. Recently, it was reported that the micropores with openings <2 nm are mainly responsible for the capture of $CO_2$, probably due to the enhanced interaction energy between $CO_2$ molecules and the adsorbent in the narrow pores.[30] Such high $CO_2$ uptake is commensurate with or higher than that of similar materials as listed in Table 3. It was clear that the PFS-800 derived from phenolic resin, with natural silk as a nitrogen source, exhibits high $CO_2$ uptakes under a facile synthesis process, which is a potential adsorbent for $CO_2$ capture at ambient pressure.

The micropore in porous carbon is the place for $CO_2$ physical adsorption.[44] The PF-K-800 was a typical microporous carbon, and its micropore surface area and volume were 1042 $m^2/g$ and 0.576 $cm^3/g$, which were higher than those of PFS-800 (749 $m^2/g$ and 0.377 $cm^3/g$) and PFS-600 (560 $m^2/g$ and 0.276 $cm^3/g$); the $CO_2$ uptake of PF-K-800 was 3.74 mmol/g


DOI: 10.1021/acssuschemeng.5b00291
ACS Sustainable Chem. Eng. 2015, 3, 1434−1442

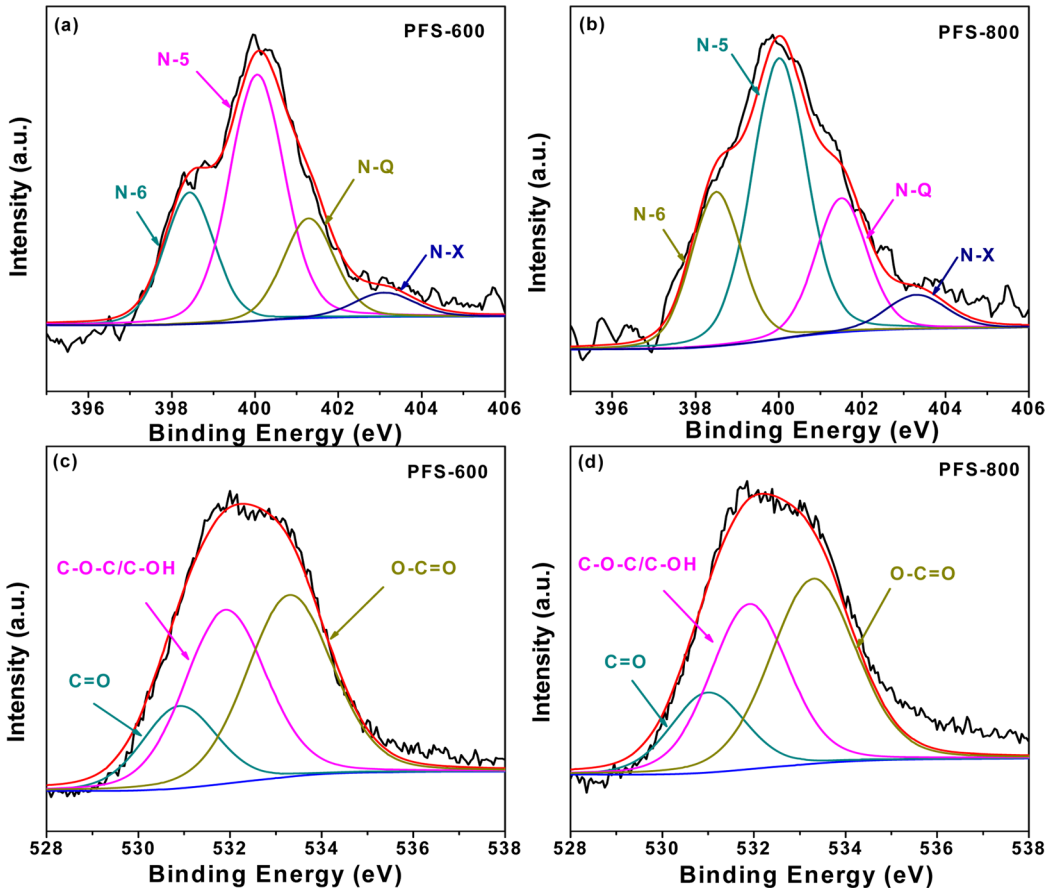


**Figure 5.** High-resolution N 1s (a, b), O 1s (c, d) XPS spectra of PFS-600 and PFS-800.

**Table 2. Binding Energy of the N 1s Species and Relative Content of Nitrogen Groups Evaluated by XPS in PFS-600 and PFS-800**

| | binding energy of N 1s species (eV) | | | | relative content of N groups (%) | | | |
|---|---|---|---|---|---|---|---|---|
| sample | N-6 | N-5 | N-Q | N-X | N-6 | N-5 | N-Q | N-X |
| PFS-800 | 398.5 | 400.0 | 401.5 | 403.3 | 24.2 | 48 | 21.4 | 6.4 |
| PFS-600 | 398.5 | 400.0 | 401.3 | 403.1 | 24.7 | 50.6 | 19.1 | 5.60 |

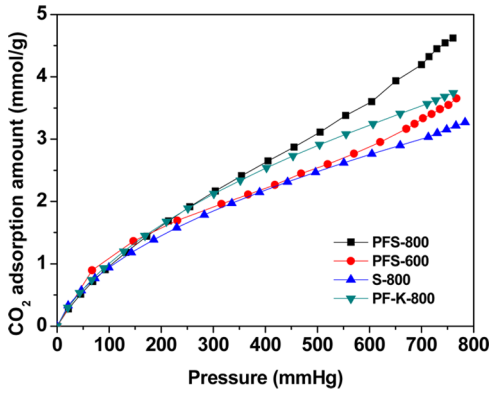


**Figure 6.** $CO_2$ sorption isotherms of PFS-600, PFS-800, PF-K-800 and S-800 at 25 °C.

at 25 °C, and it was a little higher than that of PFS-600 (3.65 mmol/g), but it was lower than that of PFS-800 (4.62 mmol/g). This suggested that the surface chemical groups also played a part in $CO_2$ adsorption. The micropore surface area and volume of PFS-800 were 2.5 times of that of PFS-600, but the $CO_2$ adsorption amount of PFS-800 was only 1.3 times of that of PFS-600. This indicated that the nitrogen-containing groups also took effect on $CO_2$ adsorption due to the higher nitrogen content of PFS-600 than that of PFS-800. As shown in Figure S4 of the Supporting Information, after acid treatment, the $CO_2$ adsorption amounts of PFS-800-HCl and PFS-600-HCl were only 3.65 and 2.60 mmol/g at ambient pressure. They decreased by 0.97 and 1.05 mmol/g compared with those of PFS-800 (4.62 mmol/g) and PFS-600 (3.65 mmol/g). Obviously, acid treatment led to ca. 20%−29% capacity loss of total $CO_2$ uptake because basic nitrogen sites were neutralized by HCl. The contributions of basic nitrogen groups and micropore to $CO_2$ uptake were estimated as 20%−30% and 80%−70%, respectively.

The isosteric heats of $CO_2$ adsorption on PFS-600, PFS-800 and PF-K-800 were obtained by adsorption isotherms at 0 and 25 °C (Figure S4 of the Supporting Information) to investigate the interaction of $CO_2$ with the carbon materials. The isosteric heats of adsorption were derived from the Clausius−Clapeyron equation:


DOI: 10.1021/acssuschemeng.5b00291
ACS Sustainable Chem. Eng. 2015, 3, 1434−1442

**Table 3. $CO_2$ Capturing Properties of Different Porous Carbon Materials**

| adsorbents | $S_{BET}$ ($m^2$/g) | N (wt %) | $CO_2$ uptake (mmol/g) | refs |
|---|---|---|---|---|
| active carbon monolith (ACM-5) | 2501 | 1.8 | 5.14 | 36 |
| N-doped templated carbon (N-TC-EMC) | 2559 | 6−7 | 4 | 37 |
| N-doped porous carbon from melamine−formaldehyde resin | 490 | 32.5 | 2.25 | 18 |
| N-doped porous carbon monolith | 467 | 1.92 | 3.13 | 23 |
| N-doped porous carbon from polyindole nanofibers | 527 | 4.17 | 3.2 | 38 |
| KQ-0.5-700 derived from urea furfural resin | 1013 | 6.71 | 4.6 | 39 |
| N-doped mesoporous carbon (IBN9) | 1181 | 12.9 | 4.5 | 40 |
| N-doped polyimine-based porous carbon | 1561 | 4.11 | 3.1 | 41 |
| N-doped mesoporous carbon from urea−formaldehyde resin | 645 | 2.37 | 3.1 | 42 |
| CDs and DVDs (mainly bisphenol A) | 2480 | 6.7 | 5.7 | 43 |
| PFS-800 from phenolic resin and silk | 1202 | 1.74 | 4.62 | this work |

$$\ln\left(\frac{P_1}{P_2}\right) = \Delta H_{ads}\left(\frac{T_1 - T_2}{R \cdot T_1 \cdot T_2}\right)$$

where $P$, $T$ and $R$ are the pressure, temperature and ideal gas constant. The curves of calculated adsorption heats are drawn in Figure 7.

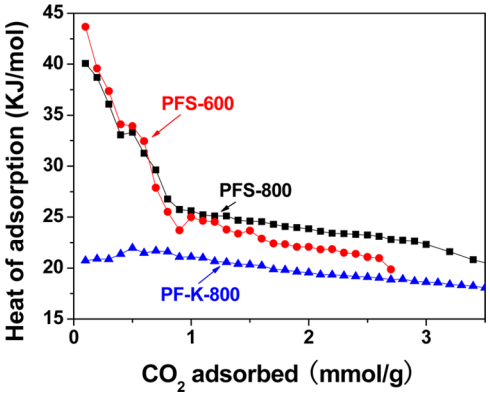


**Figure 7.** Isosteric heats of $CO_2$ adsorption on PFS-600, PFS-800 and PF-K-800 calculated by Clausius−Clapeyron equation.

The PFS-600 displayed a higher initial adsorption heat than that of PFS-800 at low $CO_2$ surface coverage because of more nitrogen-containing groups in PFS-600. According to the FT-IR analysis result and the isosteric adsorption heats of $CO_2$ on PFS-800 PFS-600, it could be deduced that chemical interactions (between N−H and $CO_2$ molecule) and polar interactions (between C−N and $CO_2$ molecule) formed between $CO_2$ and nitrogen-containing groups. For comparison, there was no nitrogen-containing group in PF-K-800; its heat of adsorption was 18−22 kJ/mol and was lower than those of PFS-600 and PFS-800. These results illustrated a stronger interaction between $CO_2$ molecule and nitrogen-containing groups on the porous carbon surface. The adsorption heats of PFS-600 and PFS-800 decreased as the $CO_2$ surface coverage increased, and it reached about 20−25 kJ/mol, which was typical physical adsorption heat for porous carbon.[45] Overall, the introduced nitrogen-containing groups into the carbon matrix caused an increase of adsorption heat indicating that the interactions between $CO_2$ molecules and nitrogen-containing groups were enhanced.

Figure 8 shows the $CO_2$-TPD profiles of PFS-600 and PFS-800. As above-discussed, the adsorption of $CO_2$ on PFS-600

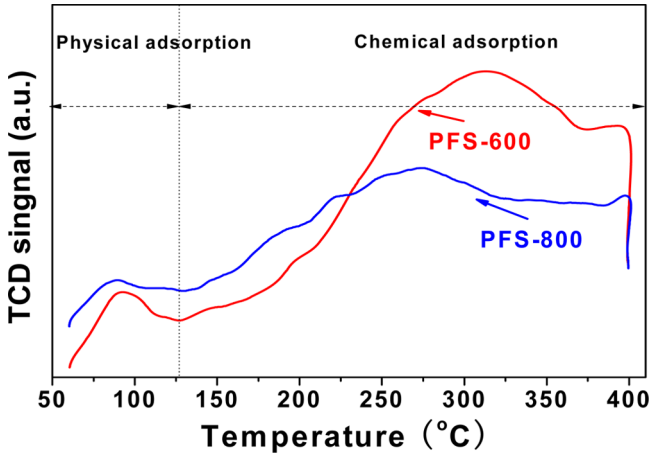


**Figure 8.** $CO_2$-TPD curves of PFS-600 and PFS-800.

and PFS-800 was composed of physical and chemical adsorption. The $CO_2$ desorbed peak of PFS-800 was higher than that of PFS-600 at lower than 230 °C due to the PFS-800 developed micropore structure, suggesting that most of the $CO_2$ molecules were physically adsorbed on PFS-800 due to its developed pore structures. In the range of 230−400 °C, the $CO_2$ desorbed peak of PFS-600 was higher than that of PFS-800 because of more nitrogen-containing chemical groups on PFS-600, which was derived from the $CO_2$ chemical adsorption, which contained the reaction of N−H groups with $CO_2$. Polar interactions between C−N groups with $CO_2$ also contributed to the $CO_2$ desorption at high temperatures. This provided another piece of proof that basic sites were also responsible for its high $CO_2$ capture performance.

The $CO_2$ adsorption reversibility on PFS-600 and PFS-800 at 25 °C has been tested for ten cycles. As illustrated in Figure 9, the $CO_2$ adsorption capabilities after ten cycles are up to 3.65 or 4.62 mmol/g for PFS-600 and PFS-800 under the same conditions at a $CO_2$ pressure of 1 atm, which indicates that they have stable $CO_2$ adsorption capabilities and excellent recyclability.

When adsorption temperature increased from 0 to 25 and 50 °C (Figure S5 of the Supporting Information), the adsorption capacities of PFS-600 decrease from 3.90 mmol/g at 0 °C to 3.56 mmol/g at 25 °C, to 1.93 mmol/g at 50 °C, and that of PFS-800 decreases from 6.46 mmol/g at 0 °C to 4.62 mmol/g at 25 °C, to 2.87 mmol/g 50 °C, respectively. In other words, the extent of decrease was expressed as a percentage of 8% from 0 to 25 °C and 51% from 25 to 50 °C for PFS-600, 26% and 53% for PFS-800, respectively. Although an increasing temperature resulted in a drastic decrease in the $CO_2$ uptake for PFS-600 and PFS-800 due to the exothermic nature of adsorption;[46] the reduced extent was different because the different content and typical nitrogen species of PFS-600 and


DOI: 10.1021/acssuschemeng.5b00291
ACS Sustainable Chem. Eng. 2015, 3, 1434−1442

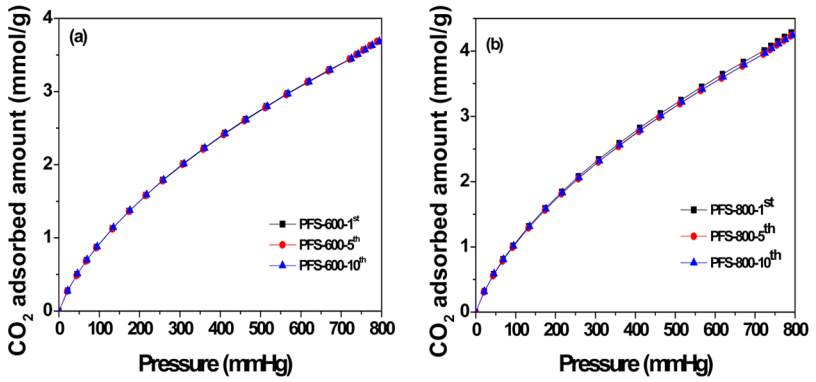


**Figure 9.** $CO_2$-multicycle-sorption isotherms for PFS-600 (a) PFS-800 (b) at 25 °C.

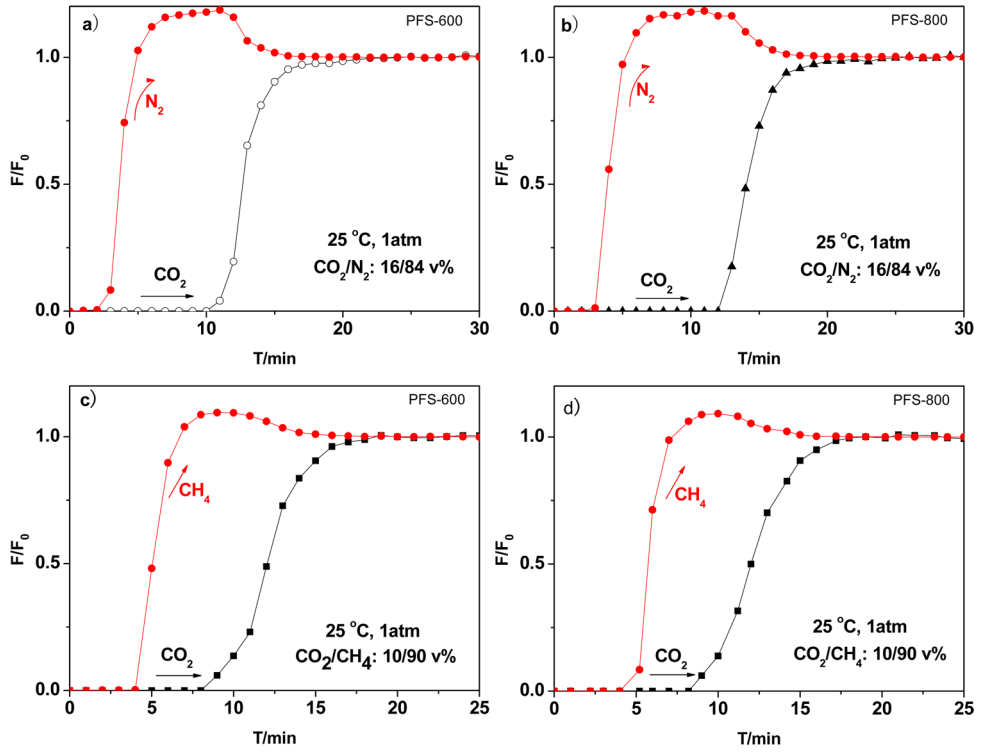


**Figure 10.** Breakthrough profiles of $CO_2$ and $N_2$, $CO_2$ and $CH_4$ on PFS-600 (a, c) and PFS-800 (b, d) under atmosphere pressure at 25 °C.

PFS-800. As shown above, the adsorption of $CO_2$ on the nitrogen-containing porous carbons consisted of physical and weak chemical adsorptions. These two types of adsorptions both occurred at lower temperatures, whereas the weak chemical adsorption played a notable role at high temperatures.

The breakthrough curves of $CO_2$ from $CO_2$−$N_2$ and $CO_2$−$CH_4$ for PFS-600 and PFS-800 were examined to investigate its separation properties, the results are demonstrated in Figure 10. Remarkably, PFS-600 and PFS-800 could dynamically separate $CO_2$ from $CO_2$−$N_2$ at 25 °C with $CO_2$ concentrations of 16 vol % (Figure 10a,b). The calculated $CO_2$ uptakes by PFS-600 and PFS-800 were 1.04 and 1.14 mmol/g, respectively. These results were well consistent with the adsorption capacities of pure $CO_2$ at 0.13 and 0.10 atm, indicating that PFS-600 and PFS-800 were extremely selective for adsorbing $CO_2$ over $N_2$. In addition, PFS-600 and PFS-800 could also dynamically separate the $CO_2$ from $CO_2$−$CH_4$ stream at 25 °C with $CO_2$ concentrations of 10 vol % (Figure 10c,d). The calculated $CO_2$ uptakes by PFS-600 and PFS-800 were 0.45 and 0.57 mmol/g, respectively. This provided a useful reference of rationally designing porous carbon for dilute $CO_2$ separation.

## CONCLUSIONS

Nitrogen-doping microporous carbon with a developed pore structure and 1.75 wt % nitrogen content was fabricated using silk as a nitrogen source and copolymer of phloroglucinol with formaldehyde as a carbon resource. KOH played roles of catalytic silk hydrolysis, phloroglucinol with glutaraldehyde polymerizing and pore forming during the activation process. Nitrogen-doping microporous carbon showed superior $CO_2$ uptakes of 6.2 and 4.34 mmol/g at 0 and 25 °C, respectively. Moreover, it is highly effective and selectively adsorbing $CO_2$ from $CO_2$−$N_2$ and $CO_2$−$CH_4$. This provided an approach to design rationally novel porous carbons as an ideal candidate for gas separation.



DOI: 10.1021/acssuschemeng.5b00291
ACS Sustainable Chem. Eng. 2015, 3, 1434−1442

## ■ ASSOCIATED CONTENT

### Supporting Information

Exhausted gases compositions, SEM images, C 1s XPS spectra, FT-IR spectra, $CO_2$ adsorption isotherms and binding energy of the O 1s species. The Supporting Information is available free of charge on the ACS Publications website at DOI: 10.1021/acssuschemeng.5b00291.

## ■ AUTHOR INFORMATION

### Corresponding Author

*W. Shen. Tel.: +86 351 4041153. E-mail: shenwzh2000@yahoo.com.

### Notes

The authors declare no competing financial interest.

## ■ ACKNOWLEDGMENTS

The authors gratefully acknowledge the financial support of this work by the National Basic Research Program of China (No. 2012CB626806), International Science & Technology Cooperation Program of China (No. 2011DFA51980), National Science Foundation of China (No. 21276266) and Shanxi Coal Based Key Scientific and Technological Project (MD2014-09).

## ■ REFERENCES

(1) Joo, S. H.; Choi, S. J.; Oh, I.; Kwak, J.; Liu, Z.; Terasaki, O.; Ryoo, R. Ordered nanoporous arrays of carbon supporting high dispersions of platinum nanoparticles. *Nature* **2001**, *412*, 169−172.

(2) Liang, C. D.; Li, Z. J.; Dai, S. Mesoporous carbon materials: Synthesis and modification. *Angew. Chem., Int. Ed.* **2008**, *47*, 3696−3717.

(3) Wan, Y.; Shi, Y. F.; Zhao, D. Y. Supramolecular aggregates as templates: Ordered mesoporous polymers and carbons. *Chem. Mater.* **2008**, *20*, 932−945.

(4) Wang, X. C.; Yu, J. C.; Hou, Y. D.; Fu, X. Z. Three-dimensionally ordered mesoporous molecular-sieve films as solid superacid photo catalysts. *Adv. Mater.* **2005**, *17* (1), 99−102.

(5) Paraknowitsch, J. P.; Zhang, J.; Su, D. S.; Thomas, A.; Antonietti, M. Ionic liquids as precursors for nitrogen-doped graphitic carbon. *Adv. Mater.* **2010**, *22*, 87−92.

(6) Lee, K. J.; Shiratori, N.; Lee, G. H.; Miyawaki, J.; Mochida, I.; Yoon, S. H.; Jang, J. Activated carbon nanofiber produced from electrospun polyacrylonitrile nanofiber as a highly efficient formaldehyde adsorbent. *Carbon* **2010**, *48*, 4248−4255.

(7) Kubota, M.; Hata, A.; Matsuda, H. Preparation of activated carbon from phenolic resin by KOH chemical activation under microwave heating. *Carbon* **2009**, *47*, 2805−2811.

(8) Demiral, H.; Gunduzoglu, G. Removal of nitrate from aqueous solutions by activated carbon prepared from sugar beet bagasse. *Bioresour. Technol.* **2010**, *101*, 1675−1680.

(9) Lillo-Rodenas, M. A.; Cazorla-Amoros, D.; Linares-Solano, A. Understanding chemical reactions between carbons and NaOH and KOH - An insight into the chemical activation mechanism. *Carbon* **2003**, *41*, 267−275.

(10) Zhu, Y. W.; Murali, S.; Stoller, M. D.; Ganesh, K. J.; Cai, W. W.; Ferreira, P. J.; Pirkle, A.; Wallace, R. M.; Cychosz, K. A.; Thommes, M.; Su, D.; Stach, E. A.; Ruoff, R. S. Carbon-based supercapacitors produced by activation of graphene. *Science* **2011**, *332*, 1537−1541.

(11) Raymundo-Pinero, E.; Azais, P.; Cacciaguerra, T.; Cazorla-Amoros, D.; Linares-Solano, A.; Beguin, F. KOH and NaOH activation mechanisms of multiwalled carbon nanotubes with different structural organisation. *Carbon* **2005**, *43*, 786−795.

(12) Jin, J.; Tanaka, S.; Egashira, Y.; Nishiyama, N. KOH activation of ordered mesoporous carbons prepared by a soft-templating method and their enhanced electrochemical properties. *Carbon* **2010**, *48*, 1985−1989.

(13) Kim, B. K.; Ryu, S. K.; Kim, B. J.; Park, S. J. Adsorption behavior of propylamine on activated carbon fiber surfaces as induced by oxygen functional complexes. *J. Colloid Interface Sci.* **2006**, *302*, 695−697.

(14) Oda, H.; Yamashita, A.; Minoura, S.; Okamoto, M.; Morimoto, T. Modification of the oxygen-containing functional group on activated carbon fiber in electrodes of an electric double-layer capacitor. *J. Power Source* **2006**, *158*, 1510−1516.

(15) El-Sayed, Y.; Bandosz, T. J. Role of surface oxygen groups in incorporation of nitrogen to activated carbons via ethylmethylamine adsorption. *Langmuir* **2005**, *21*, 1282−1289.

(16) Shen, W. Z.; Fan, W. B. Nitrogen-containing porous carbons: Synthesis and application. *J. Mater. Chem. A* **2013**, *1*, 999−1013.

(17) Shen, W. Z.; Zhang, S. C.; He, Y.; Li, J. F.; Fan, W. B. Hierarchical porous polyacrylonitrile-based activated carbon fibers for $CO_2$ capture. *J. Mater. Chem.* **2011**, *21*, 14036−14040.

(18) Pevida, C.; Drage, T. C.; Snape, C. E. Silica-templated melamine-formaldehyde resin derived adsorbents for $CO_2$ capture. *Carbon* **2008**, *46*, 1464−1474.

(19) Goettmann, F.; Fischer, A.; Antonietti, M.; Thomas, A. Chemical synthesis of mesoporous carbon nitrides using hard templates and their use as a metal-free catalyst for Friedel-Crafts reaction of benzene. *Angew. Chem., Int. Ed.* **2006**, *45*, 4467−4471.

(20) Li, Q.; Yang, J. P.; Feng, D.; Wu, Z. X.; Wu, Q. L.; Park, S. S.; Ha, C. S.; Zhao, D. Y. Facile synthesis of porous carbon nitride spheres with hierarchical three-dimensional mesostructures for $CO_2$ capture. *Nano Res.* **2010**, *3*, 632−642.

(21) Jin, Y. H.; Voss, B. A.; Jin, A.; Long, H.; Noble, R. D.; Zhang, W. Highly $CO_2$-selective organic molecular cages: What determines the $CO_2$ selectivity. *J. Am. Chem. Soc.* **2011**, *133*, 6650−6658.

(22) Fan, X. Q.; Zhang, L. X.; Zhang, G. B.; Shu, Z.; Shi, J. L. Chitosan derived nitrogen-doped microporous carbons for high performance $CO_2$ capture. *Carbon* **2013**, *61*, 423−430.

(23) Hao, G. P.; Li, W. C.; Qian, D.; Lu, A. H. Rapid synthesis of nitrogen-doped porous carbon monolith for $CO_2$ capture. *Adv. Mater.* **2010**, *22*, 853−857.

(24) Kim, H.; Kim, Y.; Yoon, M.; Linn, S.; Park, S. M.; Seo, G.; Kim, K. Highly selective carbon dioxide sorption in an organic molecular porous material. *J. Am. Chem. Soc.* **2010**, *132*, 12200−12222.

(25) Phan, A.; Doonan, C. J.; Uribe-Romo, F. J.; Knobler, C. B.; O'Keeffe, M.; Yaghi, O. M. Synthesis, structure, and carbon dioxide capture properties of zeolitic imidazolate frameworks. *Acc. Chem. Res.* **2010**, *43*, 58−67.

(26) Wen, J. J.; Gu, F. N.; Wei, F.; Zhou, Y.; Lin, W. G.; Yang, J.; Yang, J. Y.; Wang, Y.; Zou, Z. G.; Zhu, J. H. One-pot synthesis of the amine-modified meso-structured monolith $CO_2$ adsorbent. *J. Mater. Chem.* **2010**, *20*, 2840−2846.

(27) Lindmark, J.; Hedlund, J. Modification of MFI membranes with amine groups for enhanced $CO_2$ selectivity. *J. Mater. Chem.* **2010**, *20*, 2219−2225.

(28) Li, P. Y.; Ge, B. Q.; Zhang, S. J.; Chen, S. X.; Zhang, Q. K.; Zhao, Y. N. $CO_2$ capture by polyethylenimine-modified fibrous adsorbent. *Langmuir* **2008**, *24*, 6567−6574.

(29) Shen, W. Z.; Hu, T. P.; Fan, W. B. Cellulose generated-microporous carbon nanosheets with nitrogen doping. *RSC Adv.* **2014**, *4*, 9126−9132.

(30) Sevilla, M.; Valle-Vigon, P.; Fuertes, A. B. N-Doped polypyrrole-based porous carbons for $CO_2$ capture. *Adv. Funct. Mater.* **2011**, *21*, 2781−2787.

(31) Meng, Y.; Gu, D.; Zhang, F.; Shi, Y.; Cheng, L.; Feng, D.; Wu, Z. X.; Chen, Z. X.; Wan, Y.; Stein, A.; Zhao, D. Y. A family of highly ordered mesoporous polymer resin and carbon structures from organic-organic self-assembly. *Chem. Mater.* **2006**, *18*, 4447−4464.

(32) Liu, Z.; Du, Z. Y.; Song, H.; Wang, C. Y.; Subhan, F.; Xing, W.; Yan, Z. F. The fabrication of porous N-doped carbon from widely available urea formaldehyde resin for carbon dioxide adsorption. *J. Colloid Interface Sci.* **2014**, *416*, 124−132.

(33) Yu, J.; Guo, M.; Muhammad, F.; Wang, A.; Yu, G.; Ma, H.; Zhu, G. S. Simple fabrication of an ordered nitrogen-doped mesoporous

carbon with resorcinol-melamine-formaldehyde resin. *Microporous Mesoporous Mater.* **2014**, *190*, 117−127.
(34) Zhao, L.; Fan, L. Z.; Zhou, M. Q.; Guan, H.; Qiao, S.; Antonietti, M.; Titirici, M. M. Nitrogen-containing hydrothermal carbons with superior performance in supercapacitors. *Adv. Mater.* **2010**, *22*, 5202−5206.
(35) Xu, B.; Duan, H.; Chu, M.; Cao, G. P.; Yang, Y. S. Facile synthesis of nitrogen-doped porous carbon for supercapacitors. *J. Mater. Chem. A* **2013**, *1*, 4565−4570.
(36) Nandi, M.; Okada, K.; Dutta, A.; Bhaumik, A.; Maruyama, J.; Derksa, D.; Uyama, H. Unprecedented $CO_2$ uptake over highly porous N-doped activated carbon monoliths prepared by physical activation. *Chem. Commun.* **2012**, *48*, 10283−10285.
(37) Wang, L. F.; Yang, R. T. Significantly increased $CO_2$ adsorption performance of nanostructured templated carbon by tuning surface area and nitrogen doping. *J. Phys. Chem. C* **2012**, *116*, 1099−1106.
(38) Saleh, M.; Tiwari, J. N.; Kemp, K. C.; Yousuf, M.; Kim, K. S. Highly selective and stable carbon dioxide uptake in polyindole-derived microporous carbon materials. *Environ. Sci. Technol.* **2013**, *47*, 5467−5473.
(39) Liu, Z.; Du, Z. Y.; Xing, W.; Yan, Z. F. Facial synthesis of N-doped microporous carbon derived from urea furfural resin with high $CO_2$ capture capacity. *Mater. Lett.* **2014**, *117*, 273−275.
(40) Zhao, Y. F.; Zhao, L.; Yao, K. X.; Yang, Y.; Zhang, Q.; Han, Y. Novel porous carbon materials with ultrahigh nitrogen contents for selective $CO_2$ capture. *J. Mater. Chem.* **2012**, *22*, 19726−19731.
(41) Wang, J. C.; Senkovska, I.; Oschatz, M.; Lohe, M. R.; Borchardt, L.; Heerwig, A.; Liu, Q.; Kaskel, S. Highly porous nitrogen-doped polyimine-based carbons with adjustable microstructures for $CO_2$ capture. *J. Mater. Chem. A* **2013**, *1*, 10951−10961.
(42) Yu, J.; Guo, M.; Muhammad, F.; Wang, A.; Zhang, F.; Li, Q.; Zhu, G. One-pot synthesis of highly ordered nitrogen-containing mesoporous carbon with resorcinol-urea-formaldehyde resin for $CO_2$ capture. *Carbon* **2014**, *69*, 502−514.
(43) Choma, J.; Marszewski, M.; Osuchowski, L.; Jagiello, J.; Dziura, A.; Jaroniec, M. Adsorption properties of activated carbons prepared from waste CDs and DVDs. *ACS Sustainable Chem. Eng.* **2015**, *3*, 733−742.
(44) Wei, H. R.; Deng, S. B.; Hu, B. Y.; Chen, Z. H.; Wang, B.; Huang, J.; Yu, G. Granular bamboo-derived activated carbon for high $CO_2$ adsorption: The dominant role of narrow micropores. *ChemSusChem* **2012**, *5*, 2354−2360.
(45) Himeno, S.; Komatsu, T.; Fujita, S. High-pressure adsorption equilibria of methane and carbon dioxide on several activated carbons. *J. Chem. Eng. Data* **2005**, *50*, 369−376.
(46) Brandani, F.; Ruthven, D. M. The effect of water on the adsorption of $CO_2$ and $C_3H_8$ on type X zeolites. *Ind. Eng. Chem. Res.* **2004**, *43*, 8339−8344.


DOI: 10.1021/acssuschemeng.5b00291
*ACS Sustainable Chem. Eng.* 2015, 3, 1434−1442